ACS OMEGA

http://pubs.acs.org/journal/acsodf

Article

A Novel Bionic Extracellular Matrix Polymer Scaffold Enhanced by Calcium Silicate for Bone Tissue Engineering

Mei Wang, Bowen Li, Yuhua Liu,* Lin Tang, Yi Zhang, and Qiufei Xie

Cite This: *ACS Omega* 2021, 6, 35727−35737

Read Online

ACCESS | Metrics & More | Article Recommendations | Supporting Information

ABSTRACT: A novel porous calcium silicate (CS)-enhanced small intestinal submucosa (SIS) scaffold was prepared by freeze-drying to mimic the natural extracellular matrix environment for bone tissue engineering. The micro-morphology, physicochemical properties, biological characteristics, and effects on osteogenic differentiation *in vitro* were explored; the effects on promoting bone formation *in vivo* were evaluated. The composite scaffold had an ideal three-dimensional porous structure. The amount of calcium silicate played a significant role in improving mechanical properties and promoting osteogenic differentiation. The SIS/2CS scaffold promoted proliferation and osteogenic differentiation in human bone marrow mesenchymal stem cells; it also significantly increased osteogenesis *in vivo*. This novel composite polymer scaffold has potential applications in bone tissue engineering.

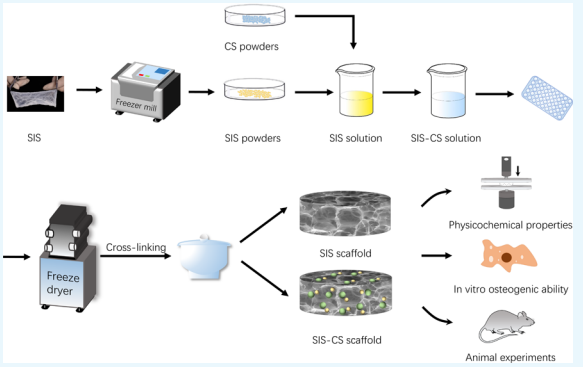

1. INTRODUCTION

There is an urgent current clinical need for an ideal bone substitute to facilitate the construction of three-dimensional porous scaffolds that consist of biocompatible and biodegradable materials for bone tissue engineering.[1−3] Inspired by the natural bone structure, an effective method to construct scaffolds for bone tissue engineering involves modification of high molecular weight polymers with inorganic substances to mimic the natural extracellular matrix (ECM) environment; this enables better cell attachment, proliferation, and differentiation.[4−6]

ECM biomaterials prepared from decellularized tissues are natural high molecular weight polymers, which have shown high bioactivity in tissue regeneration and remodeling because they have complex components and a natural tissue microstructure.[7−10] The small intestinal submucosa (SIS) is an ECM material that has been used successfully in tissue engineering.[11,12] The SIS is an excellent collagen matrix because of its natural endogenous growth factors and diverse glycosaminoglycans (GAGs).[13] Preliminary experiments confirmed the feasibility of application of SIS in bone tissue engineering.[14,15] However, SIS has some disadvantages that limit its applications in bone regeneration, such as scarcity of inorganic components and insufficient mechanical strength.

Recent studies have demonstrated effective ways to modify and enhance natural polymers by loading with active inorganic substances.[16,17] Calcium silicate (CS) ceramics are known to have greater osteoconductivity, osteoinductivity, and biocompatibility, compared with other calcium phosphate-based materials.[18,19] Silicon (Si) ions released from CS could provide an ideal environment for inducing osteogenic differentiation.[20,21] In addition, calcium (Ca) ions could react by mineralization on the surface of the scaffold, forming a hydroxyapatite (HAP) coating.[22,23] However, to our knowledge, few studies have screened and optimized CS and SIS scaffolds for osteogenesis.

A freeze-drying method was used to successfully construct a novel SIS scaffold enhanced by CS, which consisted of the excellent natural tissues of SIS and the superior components of CS. We used different concentration ratios to identify the optimal ratio of composite materials for bone tissue engineering. Analyses of physicochemical properties and mechanical strength, as well as stimulation of osteogenesis *in vitro*, were conducted to evaluate the effects of composite scaffolds. In addition, a rat skull defect model was used to evaluate the osteogenesis effect of CS-enhanced SIS scaffolds *in vivo*.

2. RESULTS

During the freeze-drying process, the mixed solution of SIS and CS was transformed into a porous sponge-like structure (Figure 1). The SIS and SIS-CS scaffolds had interconnected internal porous structures. The pores in the scaffolds were connected to each other, indicating that CS particles were scattered uniformly and attached to the SIS matrix. EDS

Received: October 8, 2021
Accepted: December 2, 2021
Published: December 17, 2021

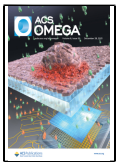

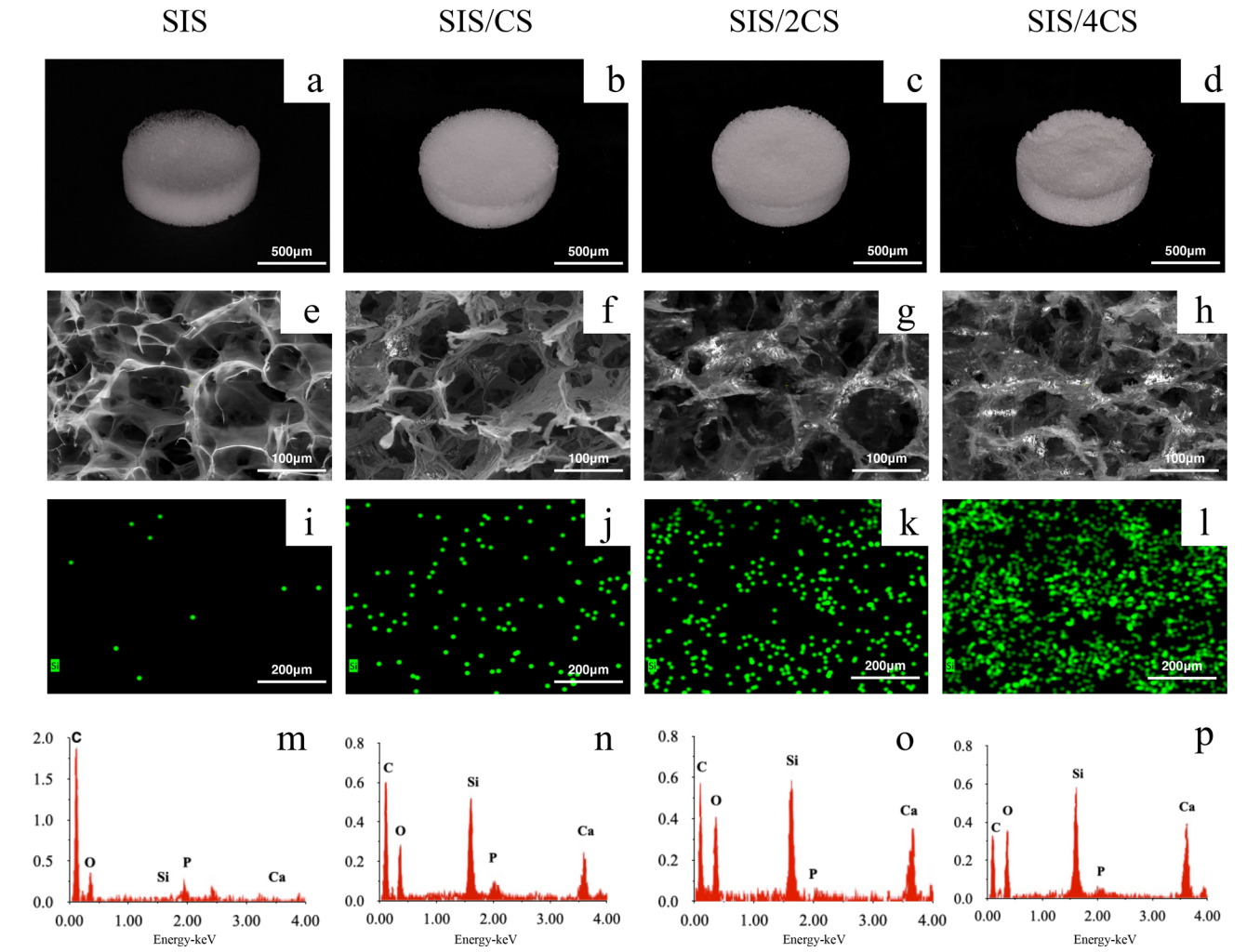

Figure 1. Structural and morphological analyses. (a−d) Overview images of SIS, SIS/CS, SIS/2CS, and SIS/4CS scaffolds. (e−h) ESEM images (1000×). (i−l) Si mapping of scaffolds. (m−p) EDS analysis of scaffolds.

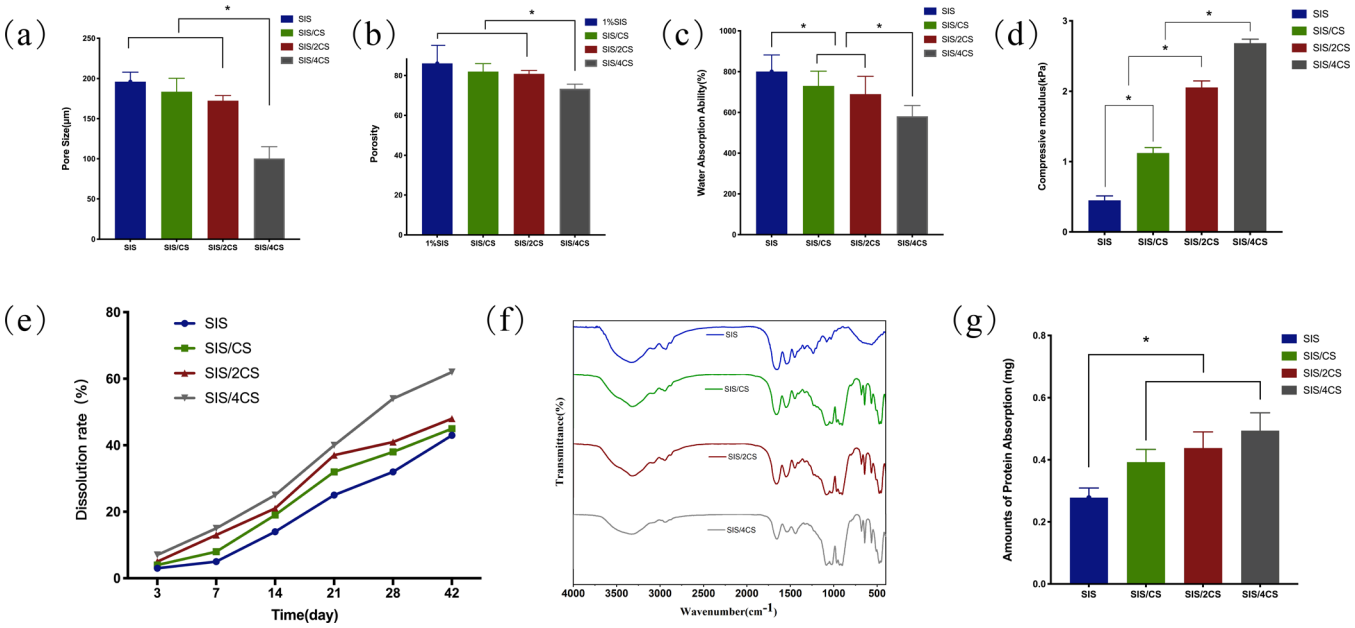

Figure 2. Structural features and analysis of physical and chemical properties. (a) Pore size. (b) Porosity. (c) Water absorption. (d) Compressive strength. (e) Degradation in PBS. (f) FTIR analysis. (g) Protein Adsorption. *, $P < 0.05$.

https://doi.org/10.1021/acsomega.1c05623
ACS Omega 2021, 6, 35727−35737

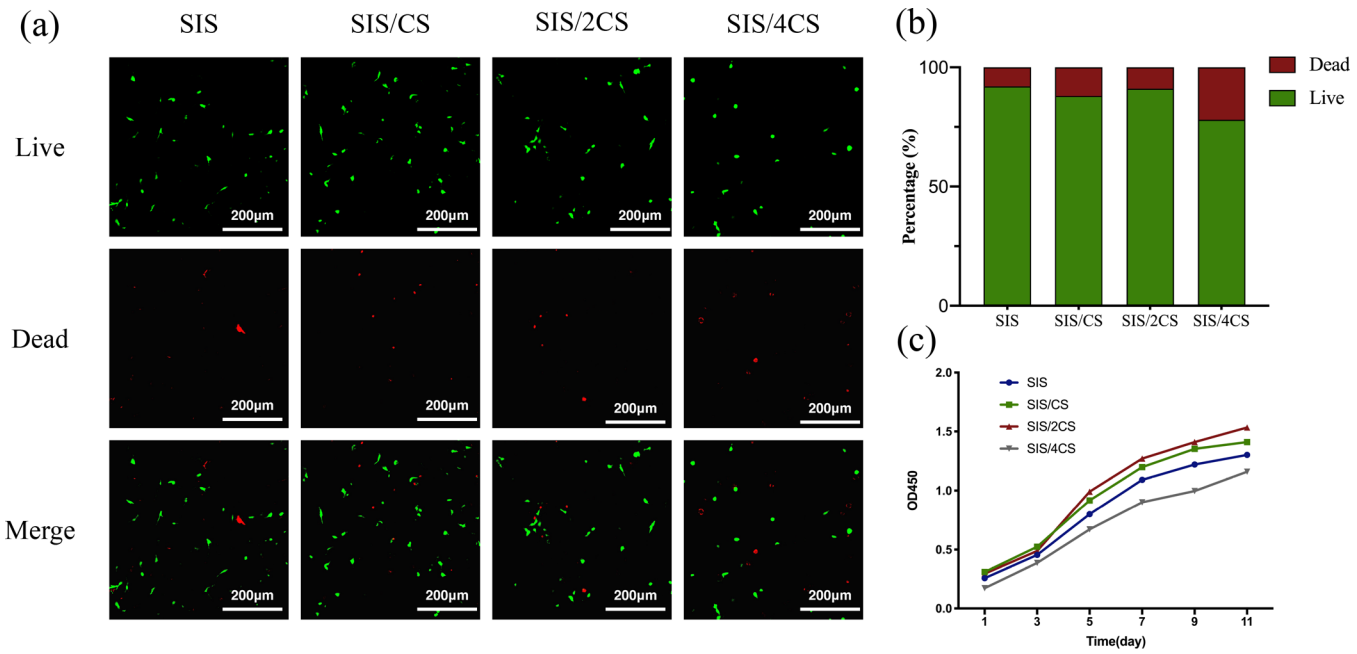

Figure 3. Biocompatibility of the scaffolds. (a) Live/dead cell staining. (b) Live/dead cell count. (c) CCK-8 cell proliferation assay.

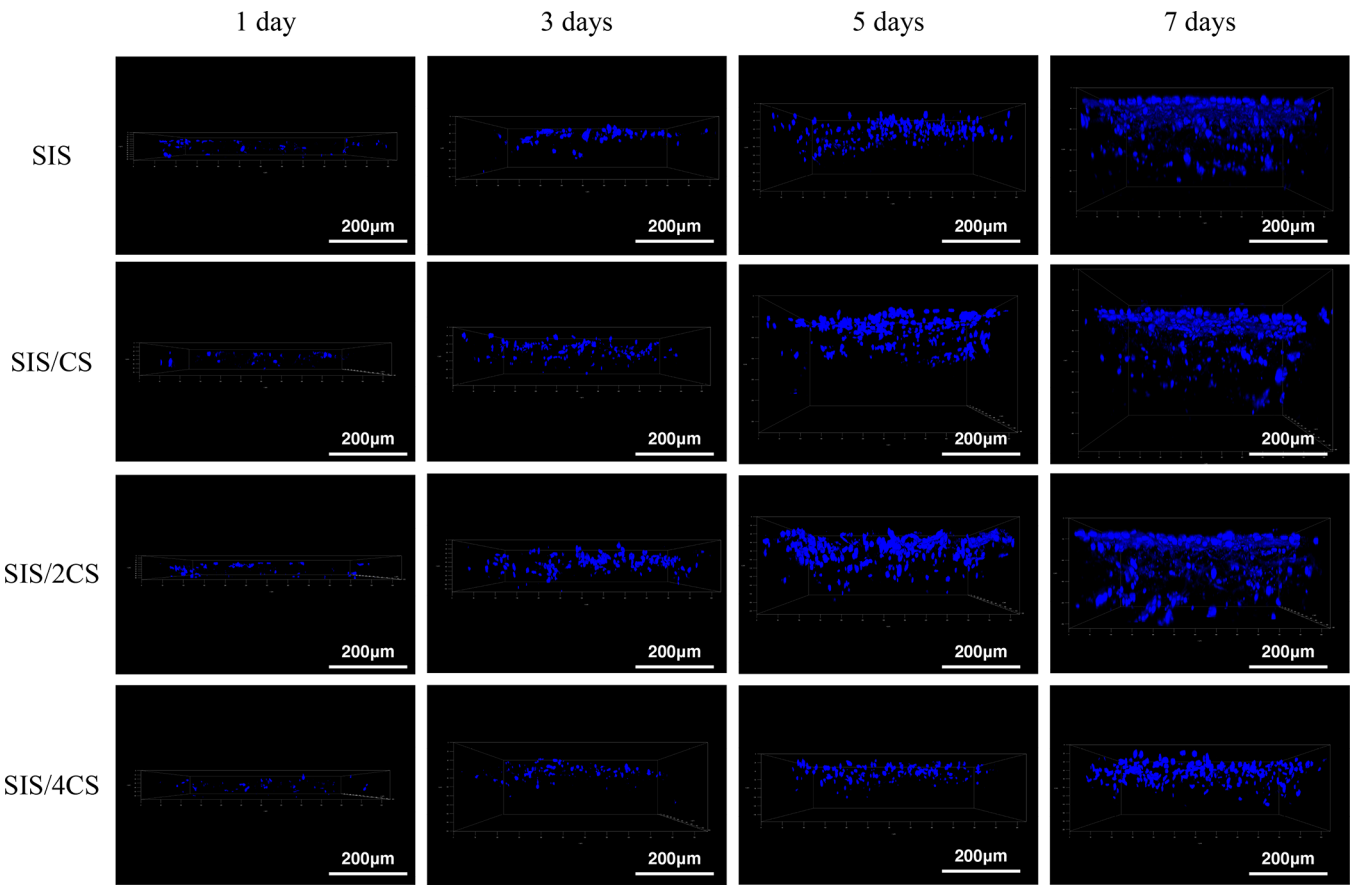

Figure 4. Observation of hBMSCs' infiltration on the scaffolds.

analysis (Figure 1m−p) showed obvious characteristic peaks for Si and Ca on the SIS/CS, SIS/2CS, and SIS/4CS scaffolds. As the CS ratio increased, Si mapping images (Figure 1i−l) revealed that the Si content increased. As Figure 2 showed, the SIS, SIS/CS, and SIS/2CS groups had high porosity and an ideal pore size for bone tissue engineering. The SIS/4CS group had significantly lower values of porosity and smaller pore size, compared with the other groups. The scaffolds exhibited satisfactory water absorption. The compressive strength of the scaffold was significantly enhanced with increases in the CS ratio (Figure 2d). The compressive strength of the SIS/2CS group was almost five times the strength of the SIS scaffold.

https://doi.org/10.1021/acsomega.1c05623
ACS Omega 2021, 6, 35727−35737

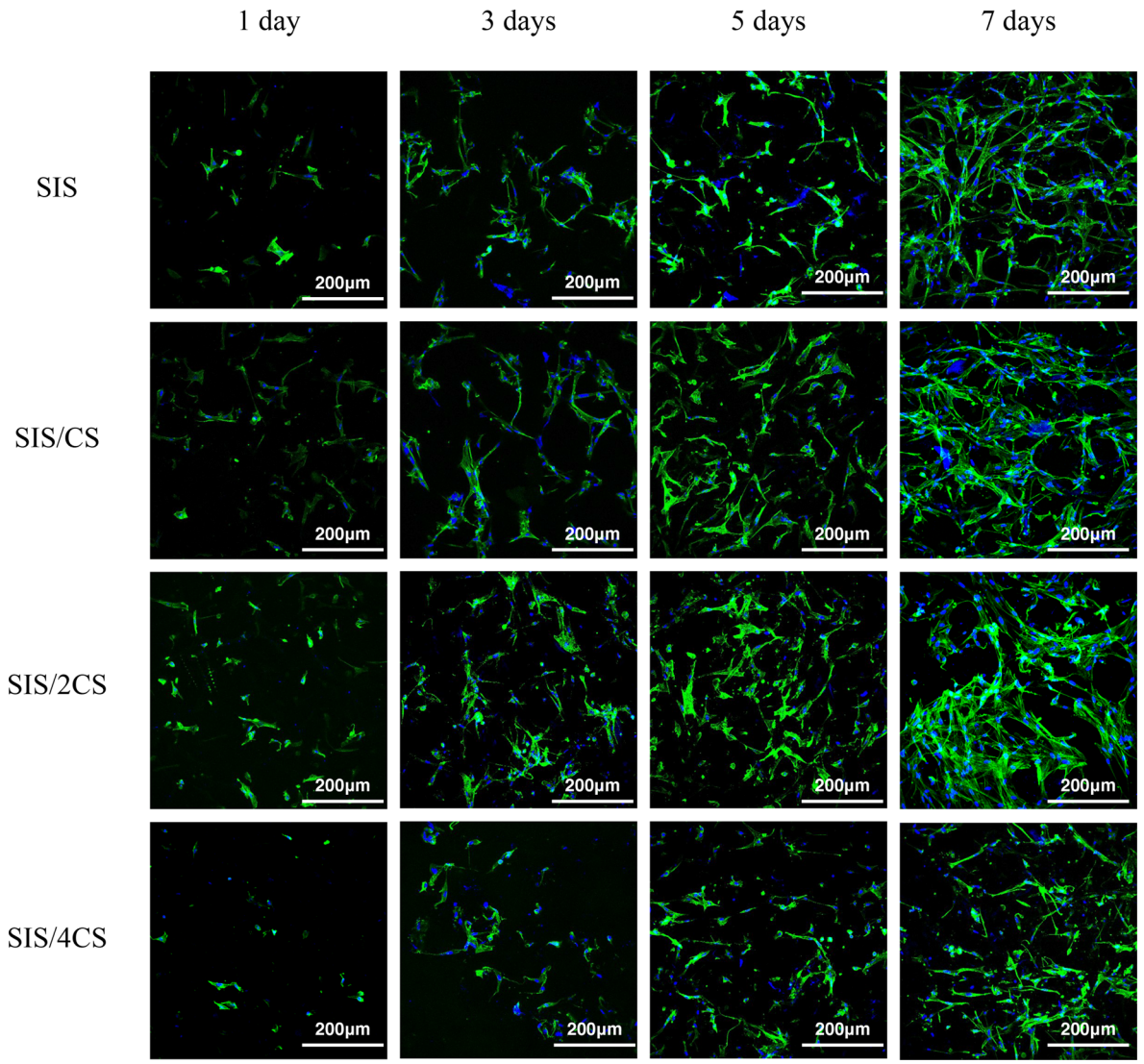

Figure 5. Observation of hBMSCs' morphology on the scaffolds.

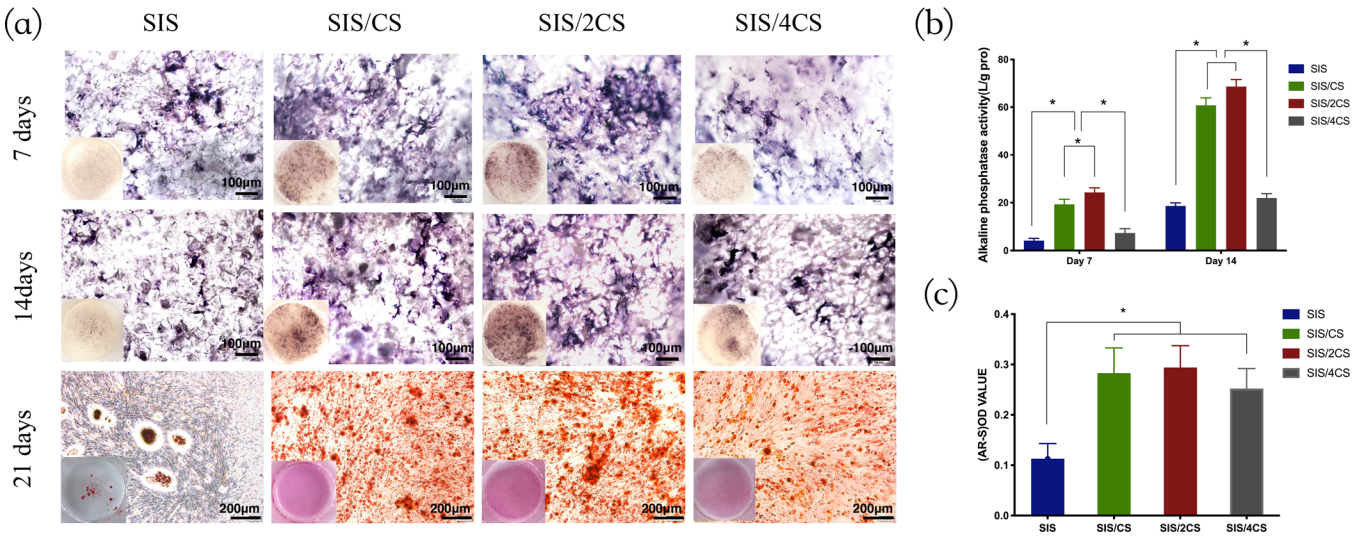

Figure 6. Osteogenic differentiation of hBMSCs. (a) ALP and alizarin red S (AR-S) staining. (b) Quantitative assessment of ALP activity. (c) Semi-quantitative assessment of AR-S findings. *, $P < 0.05$.

https://doi.org/10.1021/acsomega.1c05623
ACS Omega 2021, 6, 35727−35737

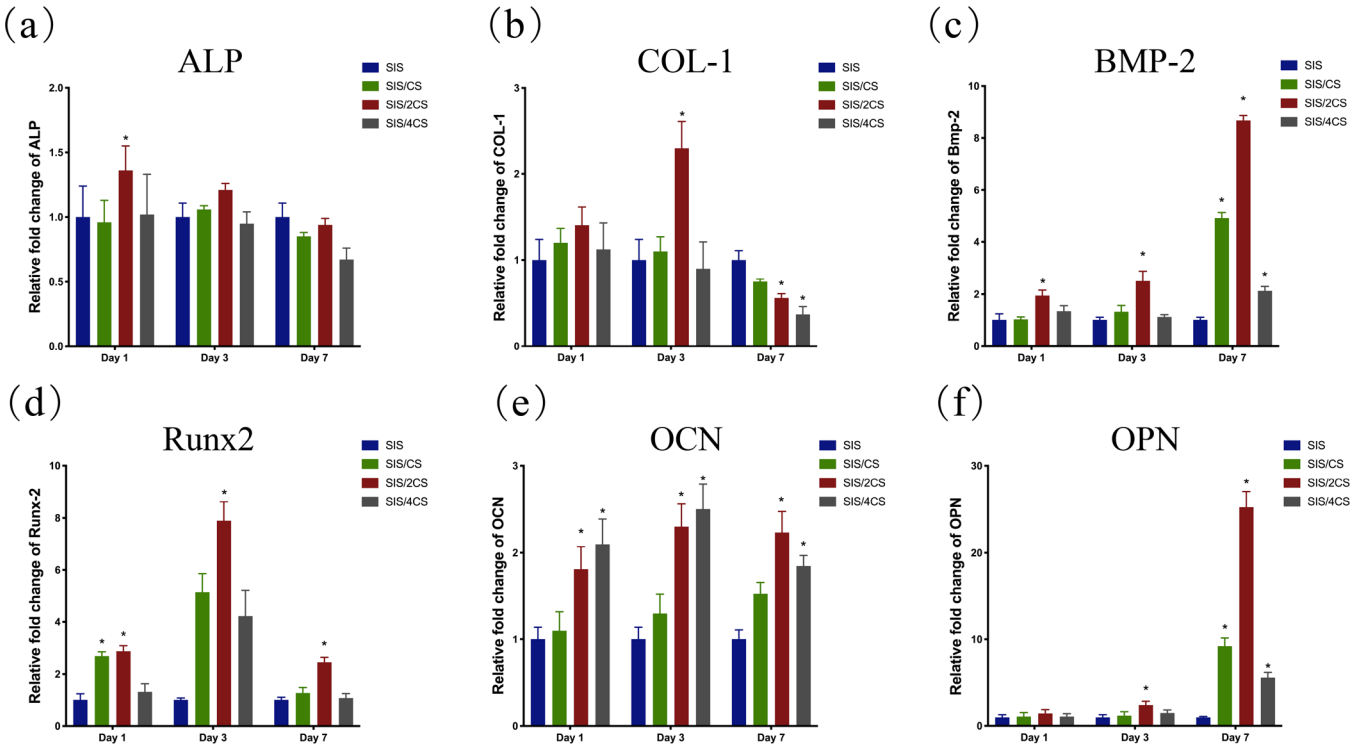

Figure 7. mRNA expression levels of the osteogenic differentiation markers (a) ALP, (b) COL-1, (c) BMP-2, (d) Runx2, (e) OCN, and (f) OPN after 1, 3, and 7 days of cell culture in osteogenic medium. *, $P < 0.05$.

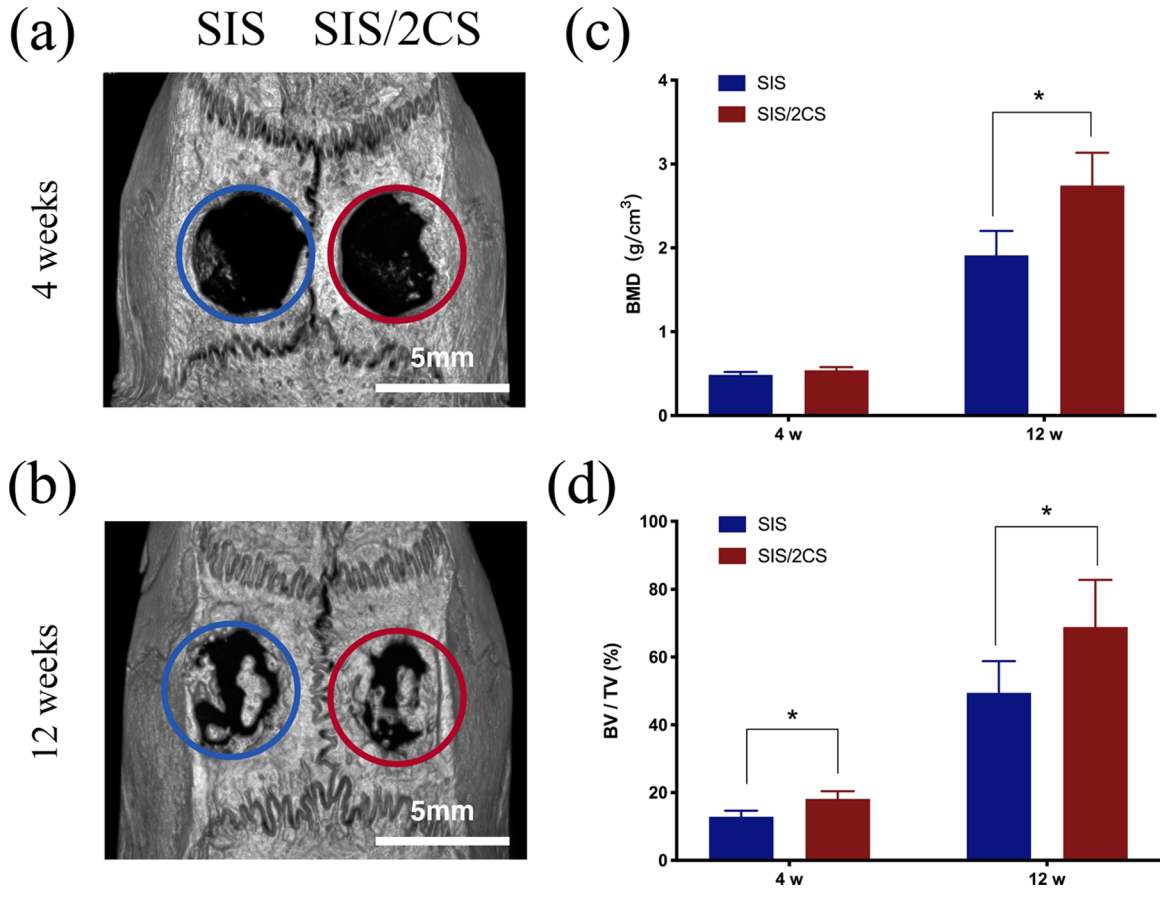

Figure 8. Micro-CT analysis. (a) Micro-CT of skull defects of the SIS and SIS/2CS scaffolds at 4 weeks. Blue, SIS group; red, SIS/2CS group. (b) Micro-CT of skull defects of the SIS and SIS/2CS scaffolds at 12 weeks. (c) Quantitative analysis of BMD. (d) Quantitative analysis of bone volume fraction (BV/TV). BMD, bone mineral density; BV, bone volume; TV, total volume. *, $P < 0.05$.

https://doi.org/10.1021/acsomega.1c05623
ACS Omega 2021, 6, 35727−35737

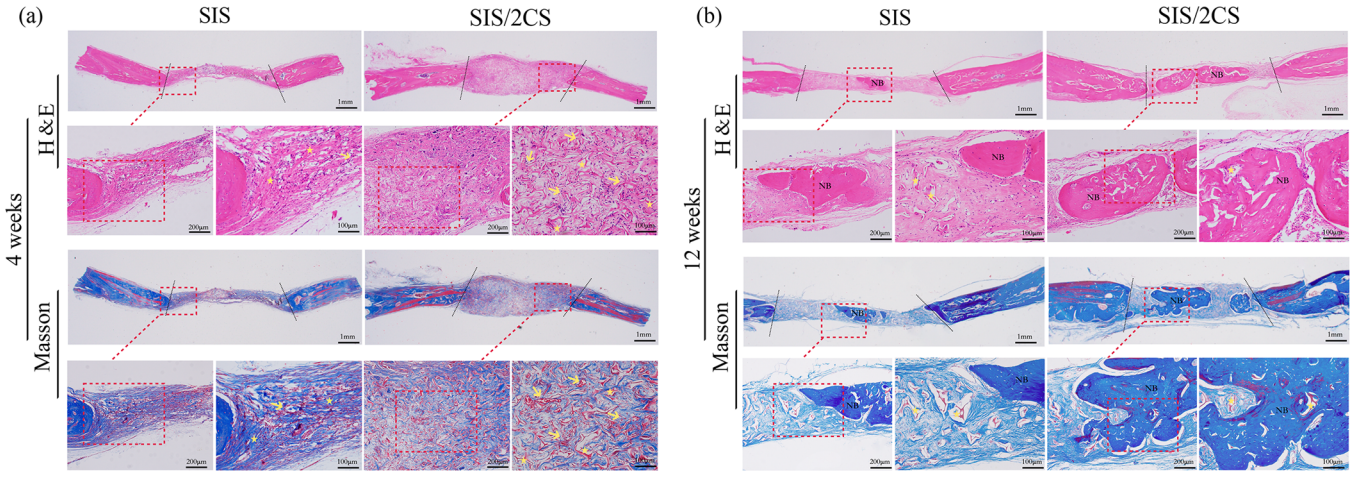

Figure 9. Histological analysis. H&E and Masson's trichrome staining of skull defects at 4 (a) and 12 weeks (b) after surgery. NB: new bone. Yellow arrow: new blood vessels. Yellow asterisk: scaffolds.

This result was similar to mechanical studies of SIS-HAP, suggesting that the addition of inorganic particles effectively improves the mechanical strength of the scaffolds, which is important to support the graft area for clinical applications.[16] The SIS/4CS scaffold showed better mechanical properties, but the dissolution loss rate was higher for the SIS/4CS scaffold in PBS than the other groups (Figure 2e). FTIR analysis (Figure 2f) confirmed the incorporation of CS into the SIS scaffold. The characteristic Si−O−Si bands of CS at 902 cm^{-1} and Si−O bands at 475 cm^{-1} were present in the spectrum.[24] Figure 2g showed that SIS and SIS-CS scaffolds could effectively adsorb proteins and the protein adsorption in SIS-CS scaffolds was significantly higher than that of the SIS scaffold.

The biocompatibility of the scaffolds was evaluated by live/dead cell staining and the CCK-8 cell proliferation assay. After co-culturing with hBMSCs for 1 day, large numbers of living cells were attached to the scaffolds in each group with a few dead cells (Figure 3). The results showed that hBMSCs proliferated well on the scaffolds, and there were no significant differences among groups ($P > 0.05$) (Figure 3c). Thus, the structure and chemical composition of the composite scaffold provided a basis for rapid cell adhesion and proliferation.

As Figure 4 showed, hBMSCs grew on the surface of the scaffolds on the first day and began to grow into the scaffold on day 3. The cells infiltrated into the scaffold, with a better ductility on days 5 and 7. As Figure 5 showed, it could be concluded that the scaffold in each group presented good cell infiltration, and the cells could grow into the scaffold through the three-dimensional interconnected pores.

Next, we evaluated the bone formation performance of the scaffold *in vitro* by examining ALP activity and AR-S staining as an indicator of ECM calcification. The osteogenic differentiation results *in vitro* on days 7 and 14 (Figure 6) showed that the SIS/CS and SIS/2CS groups had stronger staining, compared with the SIS group; the quantitative values were significantly higher for SIS/2CS scaffolds than for the other groups on day 7 ($P < 0.05$). After 21 days, the SIS/CS, SIS/2CS, and SIS/4CS groups showed stronger AR-S staining than the SIS group (Figure 6c); our semi-quantitative results were consistent with the observed staining results. We concluded that the addition of CS improved early bone formation and mineralization of the scaffolds. This study showed that the SIS/2CS group had the best bone formation effect by setting different ratios of SIS and CS. It is worth noting that this ratio was close to the ratio of organic and inorganic matter in natural human bone.[25]

The osteogenic differentiation of hBMSCs was evaluated based on the dynamic measurement of the marker genes ALP, Col-1, BMP-2, Runx2, OCN, and OPN on days 1, 3, and 7 (Figure 7). As expected, significant increases in the expression levels of these genes were observed in the SIS/2CS group at specific time points examined. The results showed that the composition and porous structure of the composite scaffold were important for osteoinduction; the SIS/2CS group exhibited the optimal bone formation effect.

New bone formation ability *in vivo* was evaluated by micro-CT analysis and histological staining. As shown in Figure 8, the bone defects in the SIS and SIS/2CS groups remained largely open at 4 weeks. However, some new bone formation within 5 mm of the defect edges was evident in the SIS/2CS group. At 12 weeks, more new bone formations and mineralizations were evident in the defect area of the SIS/2CS group. The bone volume fraction and BMD were significantly higher in the SIS/2CS scaffold than in the SIS scaffold.

Histological analyses with H&E and Masson's trichrome staining demonstrated the distribution of new bone and blood vessels. As shown in Figure 9, fibrous connective tissue and non-degraded scaffold materials occupied the bone defect area at 4 weeks, while minimal new bone was observed at the edges of the defects. The SIS/2CS group showed large numbers of new blood vessels and osteoblasts, which were important for bone regeneration. At 12 weeks, mature bone matrix was found in both SIS and SIS/2CS groups. The proportion of new bone formation was higher in the SIS/2CS group (69.88 ± 13.92%) than in the SIS group (37.50 ± 9.29%), consistent with the micro-CT findings ($P < 0.05$). There was a layer of osteoblasts on the boundary of the newly formed bone. Notably, non-degraded and red-stained material was scattered throughout some mature bone islands.

3. DISCUSSION

The natural polymer SIS retains ECM components as biological cues for cell proliferation, migration, and differentiation.[12,26] However, it differs from the microenvironment of bone in that it lacks a mineral system for inducing

https://doi.org/10.1021/acsomega.1c05623
ACS Omega 2021, 6, 35727−35737

osteogenesis; moreover, it does not have satisfactory mechanical characteristics for bone tissue engineering.[27] To develop a composite scaffold with enhanced mechanical performance and osteogenic effects for bone tissue engineering, we loaded CS onto the surface of SIS to prepare a novel CS-enhanced SIS scaffold in this study.

Networks with similar morphologies to natural matrix structures are required for bone tissue engineering scaffolds.[28,29] To prepare a CS-enhanced SIS scaffold with sufficient pore size and high porosity conducive to cell seeding and diffusion, we adopted a freeze-drying method that has been widely used for preparing natural polymer scaffolds. In this process, the model was pre-treated at a low temperature sufficient to convert interstitial water into ice crystals, which were then sublimated into water vapor at specific temperatures and pressures, thus yielding a porous scaffold.[30,31] This method involves simple treatment processes, and the low temperature may prevent damage to natural active ingredients in collagen.[32] Previous studies have shown that freeze-drying at −20 °C is suitable for obtaining appropriate pore size and porosity in bone tissue engineering.[33] In this study, the pore size in scaffolds prepared at this temperature varied from 58 to 329 μm; there is no significant difference in the pore size of SIS, SIS/CS and SIS/2CS scaffolds. The porosity was >80% for these scaffolds, which fulfilled the requirements for bone tissue engineering.[28,34,35]

Enhanced mechanical strength is one of the most important physical properties of scaffolds conferred by inorganic fillers in natural polymer substrates.[36] With satisfactory mechanical performance, the scaffolds can provide a reliable environment for cell adhesion and osteogenic differentiation.[24,37] Previous reports indicated that osteogenic differentiation can be enhanced by integrin-mediated mechanical transduction for some scaffolds with greater rigidity.[38] In this study, CS enhanced the mechanical performance of the scaffolds. SIS/CS and SIS/2CS had compressive strengths two and five times higher than the strength of SIS, respectively; the mechanical strength was approximately seven times higher in the SIS/4CS group. This study showed that increased CS significantly improved the mechanical performance, although it partially reduced both the pore size and porosity. Therefore, the amount of CS must be optimized. The SIS/CS and SIS/2CS scaffolds showed improvements in relevant mechanical performance; their pore size and porosity were not significantly reduced in comparison with the SIS scaffolds. The SIS/4CS scaffolds also showed improvements in relevant mechanical performance, but their pore size and porosity were significantly reduced. This was presumably because of the change in crystal size related to excessive amounts of inorganic filler, which may have adverse effects on osteoblast proliferation and differentiation.

Cross-linking is an effective loading mode in biofunctionalization. 1-Ethyl-3-[3-dimethylaminopropyl] carbodiimide hydrochloride (EDC) is a zero-length cross-linking agent.[39] Previous studies have shown that EDC can facilitate binding between SIS and HAP.[16] In this study, SIS-CS scaffolds were freeze-dried and EDC was then used for cross-linking; the connection between SIS and CS was achieved through the interaction of amino groups with functional groups, such as Ca^{2+} and SiO_3^{2-}. In addition, FTIR analysis confirmed changes concerning functional groups in the composite scaffolds. In the infrared spectrum of the SIS scaffold, O−H and −CH stretching vibration peaks were observed in collagen; N−H stretching vibration peaks were observed in amide A. The infrared spectrum of SIS-CS scaffolds showed a characteristic absorption peak for SiO_3^{2-} in CS. In addition, symmetrical stretching vibration peaks of the Si−O−Si bond were observed in the CS skeleton; stretching vibration peaks of the Si−O tetrahedron and Si−O bonds were also observed. These findings suggested that CS had been successfully adsorbed onto SIS.

Decellularization technology makes ECM-based materials promising as natural polymer scaffold materials.[7] Multiple studies have demonstrated the low immunogenicity of decellularized SIS.[13] It is reported that the host's response to SIS is similar to that of syngeneic tissues, the process of which is consistent with the absorption and remodeling of natural tissues.[40,41] SIS retains multiple protein binding sites in the ECM. It contains various growth factors like the basic fibroblast growth factor (bFGF), epidermal growth factor (EGF), transforming growth factor-β (TGF-β), and vascular endothelial growth factor (VEGF) that promote osteoblast proliferation and osteogenic differentiation;[13,42,43] it shows a good capacity for promoting angiogenesis and osteogenesis.[44,45] Previous studies showed that natural polymer composite bone tissue scaffolds have a significantly improved osteogenic effect, in comparison with the original biomaterials.[24,46] The introduction of inorganic fillers from natural polymer substrates may confer important physical and chemical properties on the scaffolds, such as improved surface roughness, mechanical strength, cell adhesion, proliferation, and differentiation.[47] Calcium silicate ceramics have attracted considerable attention because they have good mechanical performance; can promote osteoblast adhesion, proliferation, and differentiation; and may induce angiogenesis.[48] In comparison with β-TCP, calcium silicate may more strongly promote bone regeneration by inducing angiogenesis and mineralization in scaffolds.[25]

Some *in vitro* studies have demonstrated osteogenesis enhancement by natural polymers via active inorganic material loading. In the present study, the SIS/2CS group showed stronger ALP staining than did the other groups on days 7 and 14, suggesting that the SIS/2CS scaffold was conducive to the early osteogenic differentiation of hBMSCs. Analysis of osteogenesis-related gene expression showed that the SIS/2CS group had higher Runx2 and COL-1 expression levels on day 3, while it had higher BMP-2 and OPN expression levels on day 7; these findings suggested that the scaffold could regulate the expression of key osteogenic genes during osteogenic differentiation. Taken together, these findings confirmed that the CS-enhanced SIS scaffold had a better osteogenic effect *in vitro*. This was presumably because Ca and Si ions released from CS stimulated proliferation and osteogenic differentiation in hBMSCs.[49,50] Previous studies confirmed the positive effect of Si on osteogenic differentiation in osteoblasts; the effective Si concentration range for promoting cell adhesion, proliferation, osteogenic differentiation, and mineralization is 0.17−2.51 mM.[51,52] Overall, exploration of the effects of CS concentration on osteogenic differentiation as well as physical and chemical properties (e.g., via microstructure analysis, elemental analysis, evaluation of mechanical properties and degradation, and *in vitro* studies of biocompatibility and osteogenic differentiation) confirmed that the SIS/2CS group had the greatest capacity for osteogenic differentiation; its proportions of organic and inorganic

https://doi.org/10.1021/acsomega.1c05623
ACS Omega 2021, 6, 35727−35737

material were very close to the proportions present in natural bone tissue in the human body.

Further animal experiments were conducted with the SIS and SIS/2CS scaffolds, which demonstrated the best osteogenesis effects *in vitro*. This study showed that the CS-enhanced SIS scaffold had better osteogenic and angiogenic effects, compared with the SIS scaffold. Extensive neovascularization was observed by histological staining at 4 weeks, which suggests the presence of sufficient blood and nutrient supplies for subsequent osteogenesis.[53] Li et al. and Sun et al. previously reported similar phenomena.[24,54] At 12 weeks, the CS-enhanced SIS scaffold showed more massive bone regeneration and neovascularization. In addition to common bone formation in the defect margins, osteogenesis was observed in the central area, indicating that the scaffold could induce and accumulate osteoblasts; thus, it provided greater numbers of sites for bone formation and generated a better osteogenic effect. *In vivo* animal experiments confirmed that the CS-enhanced SIS scaffold had satisfactory osteogenic and angiogenic effects, consistent with the results of our *in vitro* analyses. In conclusion, a novel CS-enhanced SIS scaffold was constructed based on the natural ECM components and structure retained by SIS, as well as the presence of CS-supplied Ca and Si ions that were conducive to osteogenesis. Moreover, the osteogenic and angiogenic effects of the scaffold, as well as its mechanical performance, were enhanced by effective loading of CS after a combination of freeze-drying and cross-linking. This novel CS-enhanced SIS scaffold has potential for future applications in bone tissue engineering. Further studies are required to explore the mechanisms of osteogenesis induced by this scaffold.

4. CONCLUSIONS

We developed a novel three-dimensional porous SIS-CS scaffold with ideal pore size, porosity, and biocompatibility. The addition of CS enhanced the mechanical properties of the scaffold. The SIS/2CS scaffold promoted osteogenic differentiation and related gene expression in hBMSCs; it showed improved osteogenic and angiogenic effects *in vivo*. Therefore, this scaffold has potential for future applications in bone tissue engineering.

5. MATERIALS AND METHODS

5.1. Preparation of SIS and SIS-CS Scaffolds. SIS was pulverized using a freezer mill (6700; SPEX, Metuchen, NJ, USA) at −80 °C to yield SIS powder. SIS was dissolved at a concentration of 1% in deionized water with acetic acid (3% v/v) and pepsin (0.1% w/v). The mixture was stirred for 24 h. To prepare SIS-CS scaffolds, CS was added to a 1% w/v SIS solution to a final concentration of 0, 1, 2, or 4% w/v (SIS, SIS/CS, SIS/2CS, and SIS/4CS scaffolds, respectively) and stirred for 24 h. The solution was carefully poured into a mold and stored at −20 °C to allow for the formation of ice particles inside the scaffolds. The scaffolds were freeze-dried at −80 °C. Afterward, the scaffolds were cross-linked in accordance with the method reported previously and then freeze-dried.[14]

5.2. Structural Characterization. *5.2.1. Environmental Scanning Electron Microscopy (ESEM).* Each group of scaffolds was observed using an environmental scanning electron microscope (ESEM) (Quanta 200F; FEI, Hillsboro, OR, USA) at an electron acceleration voltage of 15.0 kV. Structural features of the scaffolds (pore shape, diameter, and porosity) were characterized using Image J software (NIH, Bethesda, MD, USA).

5.2.2. Energy Dispersive Spectrometer (EDS). The surface and elemental compositions of scaffolds were characterized by energy dispersive spectrometry (EDS).

5.2.3. Water Absorption. Dried scaffold samples (n = 3) were immersed in distilled water at room temperature. Samples were removed from the water and weighed again after the scaffolds had become saturated with water. The water absorption of each sample was calculated relative to its own weight.

5.2.4. Mechanical Evaluation. Cylindrical scaffolds (n = 5) 6 mm in diameter and 10 mm in height were produced for compressive mechanical testing with a universal testing machine (Instron, USA) at a speed of 1 mm/min. The compressive modulus (Ec) was calculated from the slope in the linear region of the stress−strain curve.

5.2.5. Dissolution Rate. Phosphate-buffered saline (PBS) was used to examine the dissolution rate. Each group of scaffolds (n = 3) was accurately weighed and immersed in centrifuge tubes that contained 15 mL of PBS. The tubes were incubated at a constant temperature of 37 °C with shaking at 80 rpm/min, and the buffer was replaced with fresh PBS every 2 days. Samples were removed at specified time points and accurately weighed after freeze-drying. The mass loss was determined by comparison with the initial weight.

5.2.6. Fourier Transform Infrared (FTIR). Components of composite scaffolds were characterized by Fourier transform infrared (FTIR) spectroscopy (Nicolet 6700, ThermoFisher, USA). The functional groups and binding forms of SIS and SIS-CS scaffolds were analyzed according to the characteristic peaks of FTIR spectra.

5.2.7. BSA Protein Adsorption. BSA was used as the model protein. Samples (n = 3) of equal volume were incubated in 1 mL PBS solution containing BSA (1 mg/mL) and PBS solution at room temperature. Afterward, the protein solutions were removed, and samples were washed with PBS buffer and incubated in 1% sodium dodecyl sulfate solution in distilled water (SDS, Sigma-Aldrich Chemicals) to recover proteins adsorbed to the scaffolds. Its concentrations in BSA solution (C_1) and in PBS (C_2) were assayed with a BCA assay kit on the microplate reader at 570 nm. The protein adsorption (C) was calculated using the weight of the BSA protein trapped by the scaffold as follows: $C = C_1 - C_2$.

5.3. *In Vitro* Osteogenic Ability. *5.3.1. Cell Viability.* Human bone marrow stromal cells (hBMSCs) were used in this study with approval from the Ethics Committee of Peking University Health Science Center (approval number: PKUSSIRB-202043106). HBMSCs were cultured on various scaffolds in 48-well plates (5×10^3 cells per scaffold). After 24 h, the cell viabilities on the scaffolds were evaluated by live/dead assays using a commercial kit (Invitrogen, Carlsbad, USA), in accordance with the manufacturer's instructions. Images were obtained using a fluorescence microscope (CLSM, Leica, Germany).

5.3.2. Cell Proliferation. Cell Counting Kit 8 assays (CCK-8; Dojindo, Kumamoto, Japan) were used to determine hBMSC proliferation. Cells were seeded on different scaffolds in 48-well plates (5×10^3 cells per scaffold). At specified time points after 2 h of incubation with CCK-8 solution, the absorbance at 450 nm (A_{450}) was determined using a microplate reader (NanoDrop 8000, Thermo, USA).

https://doi.org/10.1021/acsomega.1c05623
ACS Omega 2021, 6, 35727−35737

5.3.3. Cell Infiltration. HBMSCs were seeded on the surface of different scaffolds in 48-well plates (5×10^4 cells per scaffold) and cultured for 1, 3, 5, and 7 days. The cytoskeletons were stained with FITC-Phalloidin, and the nuclei were stained with 4,6-diamidino-2-phenylindole. The depth and shape of cell infiltration were observed by confocal laser scanning microscopy (TCS SP8 X,Leica, Germany).

5.3.4. Alkaline Phosphatase (ALP) Activity. Cells were seeded on scaffolds (2×10^4 cells per scaffold) and cultured for 7 or 14 days with osteogenic induction medium; ALP staining was performed using a BCIP/NBT ALP Kit (CoWin Biotech, China). Images were obtained under a microscope (BX51M, Olympus, Japan), and ALP activity was assessed using an ALP Activity Assay Kit (Jiancheng Technology, China).

5.3.5. Alizarin Red S (AR-S) Staining. At 21 days after osteoinduction, osteogenic differentiation of hBMSCs (2×10^4 cells per sample) was assessed by alizarin red S (AR-S) staining. Images were obtained under a microscope. The stained areas were then incubated in 100 mM cetylpyridinium chloride (Sigma-Aldrich, St. Louis, USA), and the absorbance at 562 nm (A_{562}) was measured.

5.3.6. Quantitative Real-Time PCR (qPCR). Cells were seeded on different scaffolds in 12-well plates (4×10^4 cells per scaffold) and then cultured for 1, 3, or 7 days with osteogenic induction medium. Total RNA was then extracted from hBMSCs using a Trizol reagent. ALP, collagen type I (COL-1), bone morphogenetic protein-2 (BMP-2), runt-related transcription factor 2 (Runx2), osteocalcin (OCN), osteopontin (OPN), and targeting glyceraldehyde-3-phosphate dehydrogenase (GAPDH) were amplified using a real-time PCR kit (SYBR, TaKaRa, China) and a real-time PCR machine (ABI 7500, Applied Biosystems, USA). The primer sequences used are listed in Table 1.

Table 1. Sequence of Primers

gene	primers (F = forward, R = reverse)
ALP	F: CTATCCTGGCTCCGTG
	R: GCTGGCAGTGGTCAGA
COL-1	F: AGAGGAAGGAAAGCGAGGAG
	R: GGACCAGCAACACCATCTG
BMP-2	F: TGACGAGGTCCTGAGCGAGTTC
	R: TGAGTGCCTGCGATACAGGTCTAG
RUNX2	F: TGGTTACTGTCATGGCGGGTA
	R: CCATTCCCACTAGGACTCCCA
OCN	F: GTGCAGAGTCCAGCAAAGGT
	R: TCAGCCAACTCGTCACAGTC
OPN	F: TGCTTGGGTTTGCAGTCTTCT
	R: CCAAACAGGCAAAAGCAAATC
GAPDH	F: GTTCGAGGACTGGTCCAAA
	R: GCCAGAGTTAAAAGCAGCC

5.4. Animal Experiments. Specific pathogen-free (SPF) male Sprague−Dawley rats (6−8 weeks old, body weight 300−350 g) were used to examine the bone regeneration effects *in vivo*. This experiment used a bilateral skull defect model in a total of eight rats with a total of 16 defects divided into two groups (SIS and SIS/2CS, $n = 4$ each), with the ipsilateral defect serving as a control in each rat. This experiment was approved by the Ethics Committee of Peking University Health Science Center.

5.4.1. Surgical Procedure. Under anesthesia with pentobarbital sodium (50 mg/kg), a circular full-thickness bone defect 5 mm in diameter was created on one side using a trephine implanter and saline for cooling. Scaffolds in the above experimental groups were implanted into the bone defects. After layered suturing and disinfection had been performed, the rats were resuscitated on a constant temperature table maintained at 37 °C. The rats were observed regularly after the operation; they were sacrificed at 4 or 12 weeks after surgery to explant the cranium.

5.4.2. Micro-Computed Tomography. After animals had been sacrificed, skull specimens were obtained and fixed in 4% paraformaldehyde. The regenerative effect of the skull defect was evaluated by micro-computed tomography (micro-CT). CT analysis software was used to analyze bone mineral density (BMD) and bone volume fraction (bone volume/total volume, BV/TV) to calculate new bone formation according to the extent and size of the defect area.

5.4.3. Histological Staining. After micro-CT, specimens were decalcified, embedded, and cut into 5 μm-thick sections for histological analysis with hematoxylin and eosin (H&E) and Masson's trichrome staining. Staining images were obtained under a microscope.

5.5. Statistical Analysis. Data were analyzed by two-way analysis of variance (ANOVA) and the least-significant difference (LSD) test using SPSS 26.0 software (IBM Corp, USA). In all analyses, $P < 0.05$ was considered to indicate statistical significance.

■ ASSOCIATED CONTENT

Supporting Information

The Supporting Information is available free of charge at https://pubs.acs.org/doi/10.1021/acsomega.1c05623.

New bone formation in H&E staining (Figure S1) (PDF)

■ AUTHOR INFORMATION

Corresponding Author

Yuhua Liu − *Department of Prosthodontics, Peking University School and Hospital of Stomatology & National Center of Stomatology &National Clinical Research Center for Oral Diseases & National Engineering Laboratory for Digital and Material Technology of Stomatology, Beijing 100081, China;* orcid.org/0000-0002-0043-9369; Email: liuyuhua@bjmu.edu.cn

Authors

Mei Wang − *Department of Prosthodontics, Peking University School and Hospital of Stomatology & National Center of Stomatology &National Clinical Research Center for Oral Diseases & National Engineering Laboratory for Digital and Material Technology of Stomatology, Beijing 100081, China*

Bowen Li − *Department of Prosthodontics, Peking University School and Hospital of Stomatology & National Center of Stomatology &National Clinical Research Center for Oral Diseases & National Engineering Laboratory for Digital and Material Technology of Stomatology, Beijing 100081, China*

Lin Tang − *Department of Prosthodontics, Peking University School and Hospital of Stomatology & National Center of Stomatology &National Clinical Research Center for Oral Diseases & National Engineering Laboratory for Digital and Material Technology of Stomatology, Beijing 100081, China*

Yi Zhang − *Department of General Dentistry II, Peking University School and Hospital of Stomatology & National*

https://doi.org/10.1021/acsomega.1c05623
ACS Omega 2021, 6, 35727−35737

Center of Stomatology &National Clinical Research Center for Oral Diseases & National Engineering Laboratory for Digital and Material Technology of Stomatology, Beijing 100081, China

Qiufei Xie − *Department of Prosthodontics, Peking University School and Hospital of Stomatology & National Center of Stomatology &National Clinical Research Center for Oral Diseases & National Engineering Laboratory for Digital and Material Technology of Stomatology, Beijing 100081, China*

Complete contact information is available at: https://pubs.acs.org/10.1021/acsomega.1c05623

Notes

The authors declare no competing financial interest.

■ ACKNOWLEDGMENTS

The authors acknowledge Datsing Biological Technology Co., Ltd., for kindly providing SIS materials.

■ REFERENCES

(1) Li, L.; Lu, H.; Zhao, Y.; Luo, J.; Yang, L.; Liu, W.; He, Q. Functionalized cell-free scaffolds for bone defect repair inspired by self-healing of bone fractures: A review and new perspectives. *Mater. Sci. Eng., C.* **2019**, *98*, 1241−1251.

(2) Ho-Shui-Ling, A.; Bolander, J.; Rustom, L. E.; Johnson, A. W.; Luyten, F. P.; Picart, C. Bone regeneration strategies: Engineered scaffolds, bioactive molecules and stem cells current stage and future perspectives. *Biomaterials* **2018**, *180*, 143−162.

(3) Kim, H. D.; Amirthalingam, S.; Kim, S. L.; Lee, S. S.; Rangasamy, J.; Hwang, N. S. Biomimetic Materials and Fabrication Approaches for Bone Tissue Engineering. *Adv. Healthcare Mater.* **2017**, *6*, 1700612.

(4) Huang, J.; Ratnayake, J.; Ramesh, N.; Dias, G. J. Development and Characterization of a Biocomposite Material from Chitosan and New Zealand-Sourced Bovine-Derived Hydroxyapatite for Bone Regeneration. *ACS Omega* **2020**, *5*, 16537−16546.

(5) Zhang, W.; Ling, C.; Li, X.; Sheng, R.; Liu, H.; Zhang, A.; Jiang, Y.; Chen, J.; Yao, Q. Cell-Free Biomimetic Scaffold with Cartilage Extracellular Matrix-Like Architectures for in Situ Inductive Regeneration of Osteochondral Defects. *ACS Biomater. Sci. Eng.* **2020**, *6*, 6917−6925.

(6) Fernandez-Yague, M. A.; Abbah, S. A.; McNamara, L.; Zeugolis, D. I.; Pandit, A.; Biggs, M. J. Biomimetic approaches in bone tissue engineering: Integrating biological and physicomechanical strategies. *Adv. Drug Delivery Rev.* **2015**, *84*, 1−29.

(7) Yi, S.; Ding, F.; Gong, L.; Gu, X. Extracellular Matrix Scaffolds for Tissue Engineering and Regenerative Medicine. *Curr. Stem Cell Res. Ther.* **2017**, *12*, 233−246.

(8) Preethi Soundarya, S.; Haritha Menon, A.; Viji Chandran, S.; Selvamurugan, N. Bone tissue engineering: Scaffold preparation using chitosan and other biomaterials with different design and fabrication techniques. *Int. J. Biol. Macromol.* **2018**, *119*, 1228−1239.

(9) Bakhtiar, H.; Pezeshki-Modaress, M.; Kiaipour, Z.; Shafiee, M.; Ellini, M. R.; Mazidi, A.; Rajabi, S.; Zamanlui Benisi, S.; Ostad, S. N.; Galler, K.; Pakshir, P.; Azarpazhooh, A.; Kishen, A. Pulp ECM-derived macroporous scaffolds for stimulation of dental-pulp regeneration process. *Dent. Mater.* **2020**, *36*, 76−87.

(10) Yao, Q.; Zheng, Y. W.; Lan, Q. H.; Kou, L.; Xu, H. L.; Zhao, Y. Z. Recent development and biomedical applications of decellularized extracellular matrix biomaterials. *Mater. Sci. Eng., C* **2019**, *104*, 109942.

(11) Li, M.; Zhang, C.; Cheng, M.; Gu, Q.; Zhao, J. Small intestinal submucosa: A potential osteoconductive and osteoinductive biomaterial for bone tissue engineering. *Mater. Sci. Eng., C* **2017**, *75*, 149−156.

(12) Cao, G.; Huang, Y.; Li, K.; Fan, Y.; Xie, H.; Li, X. Small intestinal submucosa: superiority, limitations and solutions, and its potential to address bottlenecks in tissue repair. *J. Mater. Chem. B* **2019**, *7*, 5038−5055.

(13) Ji, Y.; Zhou, J.; Sun, T.; Tang, K.; Xiong, Z.; Ren, Z.; Yao, S.; Chen, K.; Yang, F.; Zhu, F.; Guo, X. Diverse preparation methods for small intestinal submucosa (SIS): Decellularization, components, and structure. *J. Biomed. Mater. Res., Part A* **2019**, *107*, 689−697.

(14) Li, B.; Liu, Y.; Zhou, Y.; You, P.; Wang, M.; Tang, L.; Deng, Y. Development of a novel extracellular matrix membrane with an asymmetric structure for guided bone regeneration. *Mater. Lett.* **2020**, *274*, 127926.

(15) Wu, W.; Li, B.; Liu, Y.; Wang, X.; Tang, L. Effect of Multilaminate Small Intestinal Submucosa as a Barrier Membrane on Bone Formation in a Rabbit Mandible Defect Model. *BioMed Res. Int.* **2018**, *2018*, 3270293.

(16) Castilla Bolaños, M. A.; Buttigieg, J.; Briceño Triana, J. C. Development and characterization of a novel porous small intestine submucosa-hydroxyapatite scaffold for bone regeneration. *Mater. Sci. Eng., C* **2017**, *72*, 519−525.

(17) Singh, B. N.; Veeresh, V.; Mallick, S. P.; Jain, Y.; Sinha, S.; Rastogi, A.; Srivastava, P. Design and evaluation of chitosan/chondroitin sulfate/nano-bioglass based composite scaffold for bone tissue engineering. *Int. J. Biol. Macromol.* **2019**, *133*, 817−830.

(18) Lee, B. N.; Hong, J. U.; Kim, S. M.; Jang, J. H.; Chang, H. S.; Hwang, Y. C.; Hwang, I. N.; Oh, W. M. Anti-inflammatory and Osteogenic Effects of Calcium Silicate-based Root Canal Sealers. *J. Endod.* **2019**, *45*, 73−78.

(19) Zheng, A.; Cao, L.; Liu, Y.; Wu, J.; Zeng, D.; Hu, L.; Zhang, X.; Jiang, X. Biocompatible silk/calcium silicate/sodium alginate composite scaffolds for bone tissue engineering. *Carbohydr. Polym.* **2018**, *199*, 244−255.

(20) Weng, L.; Boda, S. K.; Teusink, M. J.; Shuler, F. D.; Li, X.; Xie, J. Binary Doping of Strontium and Copper Enhancing Osteogenesis and Angiogenesis of Bioactive Glass Nanofibers while Suppressing Osteoclast Activity. *ACS Appl. Mater. Interfaces* **2017**, *9*, 24484−24496.

(21) Narayan, R.; Agarwal, T.; Mishra, D.; Maji, S.; Mohanty, S.; Mukhopadhyay, A.; Maiti, T. K. Ectopic vascularized bone formation by human mesenchymal stem cell microtissues in a biocomposite scaffold. *Colloids Surf., B* **2017**, *160*, 661−670.

(22) Liu, W.; Zhang, G.; Wu, J.; Zhang, Y.; Liu, J.; Luo, H.; Shao, L. Insights into the angiogenic effects of nanomaterials: mechanisms involved and potential applications. *J. Nanobiotechnol.* **2020**, *18*, 9.

(23) Su, C. J.; Tu, M. G.; Wei, L. J.; Hsu, T. T.; Kao, C. T.; Chen, T. H.; Huang, T. H. Calcium Silicate/Chitosan-Coated Electrospun Poly (Lactic Acid) Fibers for Bone Tissue Engineering. *Materials* **2017**, *10*, 501.

(24) Sun, T.; Liu, M.; Yao, S.; Ji, Y.; Xiong, Z.; Tang, K.; Chen, K.; Yang, H.; Guo, X. Biomimetic Composite Scaffold Containing Small Intestinal Submucosa and Mesoporous Bioactive Glass Exhibits High Osteogenic and Angiogenic Capacity. *Tissue Eng., Part A* **2018**, *24*, 1044−1056.

(25) Li, T.; Peng, M.; Yang, Z.; Zhou, X.; Deng, Y.; Jiang, C.; Xiao, M.; Wang, J. 3D-printed IFN-γ-loading calcium silicate-β-tricalcium phosphate scaffold sequentially activates M1 and M2 polarization of macrophages to promote vascularization of tissue engineering bone. *Acta Biomater.* **2018**, *71*, 96−107.

(26) Sicari, B. M.; Dziki, J. L.; Siu, B. F.; Medberry, C. J.; Dearth, C. L.; Badylak, S. F. The promotion of a constructive macrophage phenotype by solubilized extracellular matrix. *Biomaterials* **2014**, *35*, 8605−8612.

(27) Yang, L.; Zhou, J.; Yu, K.; Yang, S.; Sun, T.; Ji, Y.; Xiong, Z.; Guo, X. Surface modified small intestinal submucosa membrane manipulates sequential immunomodulation coupled with enhanced angio- and osteogenesis towards ameliorative guided bone regeneration. *Mater. Sci. Eng., C.* **2021**, *119*, 111641.

(28) Iviglia, G.; Kargozar, S.; Baino, F. Biomaterials, current strategies, and novel nano-technological approaches for periodontal regeneration. *J. Funct. Biomater.* **2019**, *10*, 3.

(29) Zhao, Y.; Tan, K.; Zhou, Y.; Ye, Z.; Tan, W. S. A combinatorial variation in surface chemistry and pore size of three-dimensional porous poly(ε-caprolactone) scaffolds modulates the behaviors of mesenchymal stem cells. *Mater. Sci. Eng., C* **2016**, *59*, 193−202.
(30) Kim, M. S.; Hong, K. D.; Shin, H. W.; Kim, S. H.; Kim, S. H.; Lee, M. S.; Jang, W. Y.; Khang, G.; Lee, H. B. Preparation of porcine small intestinal submucosa sponge and their application as a wound dressing in full-thickness skin defect of rat. *Int. J. Biol. Macromol.* **2005**, *36*, 54−60.
(31) Roseti, L.; Parisi, V.; Petretta, M.; Cavallo, C.; Desando, G.; Bartolotti, I.; Grigolo, B. Scaffolds for bone tissue engineering: State of the art and new perspectives. *Mater. Sci. Eng., C* **2017**, *78*, 1246−1262.
(32) Soffer-Tsur, N.; Peer, D.; Dvir, T. ECM-based macroporous sponges release essential factors to support the growth of hematopoietic cells. *J. Controlled Release* **2017**, *257*, 84−90.
(33) Grenier, J.; Duval, H.; Barou, F.; Lv, P.; David, B.; Letourneur, D. Mechanisms of pore formation in hydrogel scaffolds textured by freeze-drying. *Acta Biomater.* **2019**, *94*, 195−203.
(34) Chen, G.; Kawazoe, N. Porous Scaffolds for Regeneration of Cartilage, Bone and Osteochondral Tissue. *Adv. Exp. Med. Biol.* **2018**, *1058*, 171−191.
(35) Abbasi, N.; Hamlet, S.; Love, R. M.; Nguyen, N. Porous scaffolds for bone regeneration. *J. Sci.: Adv. Mater. Devices* **2020**, *5*, 1−9.
(36) Zhao, H.; Liao, J.; Wu, F.; Shi, J. Mechanical strength improvement of chitosan/hydroxyapatite scaffolds by coating and cross-linking. *J. Mech. Behav. Biomed. Mater.* **2021**, *114*, 104169.
(37) Hamvar, M.; Bakhsheshi-Rad, H. R.; Omidi, M.; Ismail, A. F.; Aziz, M.; Berto, F.; Chen, X. Biocompatibility and bioactivity of hardystonite-based nanocomposite scaffold for tissue engineering applications. *Biomed. Phys. Eng. Express* **2020**, *6*, No. 035011.
(38) Boettiger, D. Mechanical control of integrin-mediated adhesion and signaling. *Curr. Opin. Cell Biol.* **2012**, *24*, 592−599.
(39) Bax, D. V.; Davidenko, N.; Gullberg, D.; Hamaia, S. W.; Farndale, R. W.; Best, S. M.; Cameron, R. E. Fundamental insight into the effect of carbodiimide crosslinking on cellular recognition of collagen-based scaffolds. *Acta Biomater.* **2017**, *49*, 218−234.
(40) McPherson, T. B.; Liang, H.; Record, R. D.; Badylak, S. F. Galalpha (1,3) Gal epitope in porcine small intestinal submucosa. *Tissue Eng.* **2000**, *6*, 233−239.
(41) Allman, A. J.; McPherson, T. B.; Badylak, S. F.; Merrill, L. C.; Kallakury, B.; Sheehan, C.; Raeder, R. H.; Metzger, D. W. Xenogeneic extracellular matrix grafts elicit a TH2-restricted immune response. *Transplantation* **2001**, *71*, 1631−1640.
(42) Luo, J. C.; Chen, W.; Chen, X. H.; Qin, T. W.; Huang, Y. C.; Xie, H. Q.; Li, X. Q.; Qian, Z. Y.; Yang, Z. M. A multi-step method for preparation of porcine small intestinal submucosa (SIS). *Biomaterials* **2011**, *32*, 706−713.
(43) Wang, W.; Zhang, X.; Chao, N. N.; Qin, T. W.; Ding, W.; Zhang, Y.; Sang, J. W.; Luo, J. C. Preparation and characterization of pro-angiogenic gel derived from small intestinal submucosa. *Acta Biomater.* **2016**, *29*, 135−148.
(44) Zhao, P.; Li, X.; Fang, Q.; Wang, F.; Ao, Q.; Wang, X.; Tian, X.; Tong, H.; Bai, S.; Fan, J. Surface modification of small intestine submucosa in tissue engineering. *Regener. Biomater.* **2020**, *7*, 339−348.
(45) Li, M.; Zhang, C.; Mao, Y.; Zhong, Y.; Zhao, J. A Cell-Engineered Small Intestinal Submucosa-Based Bone Mimetic Construct for Bone Regeneration. *Tissue Eng., Part A* **2018**, *24*, 1099−1111.
(46) Bharadwaz, A.; Jayasuriya, A. C. Recent trends in the application of widely used natural and synthetic polymer nanocomposites in bone tissue regeneration. *Mater. Sci. Eng., C* **2020**, *110*, 110698.
(47) Yi, L. J.; Li, J. F.; Ma, M. G.; Zhu, Y. J. Nanostructured Calcium-based Biomaterials and their Application in Drug Delivery. *Curr. Med. Chem.* **2020**, *27*, 5189−5212.
(48) Prati, C.; Gandolfi, M. G. Calcium silicate bioactive cements: Biological perspectives and clinical applications. *Dent. Mater.* **2015**, *31*, 351−370.
(49) Dong, M.; Jiao, G.; Liu, H.; Wu, W.; Li, S.; Wang, Q.; Xu, D.; Li, X.; Liu, H.; Chen, Y. Biological Silicon Stimulates Collagen Type 1 and Osteocalcin Synthesis in Human Osteoblast-Like Cells Through the BMP-2/Smad/RUNX2 Signaling Pathway. *Biol. Trace Elem. Res.* **2016**, *173*, 306−315.
(50) Shuai, C.; Guo, W.; Gao, C.; Yang, Y.; Xu, Y.; Liu, L.; Qin, T.; Sun, H.; Yang, S.; Feng, P.; Wu, P. Calcium Silicate Improved Bioactivity and Mechanical Properties of Poly(3-hydroxybutyrate-co-3-hydroxyvalerate) Scaffolds. *Polymer* **2017**, *9*, 175.
(51) Gong, T.; Wang, Z.; Zhang, Y.; Zhang, Y.; Hou, M.; Liu, X.; Wang, Y.; Zhao, L.; Ruse, N. D.; Troczynski, T.; Häfeli, U. O. A Comprehensive Study of Osteogenic Calcium Phosphate Silicate Cement: Material Characterization and In Vitro/In Vivo Testing. *Adv. Healthcare Mater.* **2016**, *5*, 457−466.
(52) Liao, F.; Peng, X. Y.; Yang, F.; Ke, Q. F.; Zhu, Z. H.; Guo, Y. P. Gadolinium-doped mesoporous calcium silicate/chitosan scaffolds enhanced bone regeneration ability. *Mater. Sci. Eng., C* **2019**, *104*, 10999.
(53) Diomede, F.; Marconi, G. D.; Fonticoli, L.; Pizzicanella, J.; Merciaro, I.; Bramanti, P.; Mazzon, E.; Trubiani, O. Functional Relationship between Osteogenesis and Angiogenesis in Tissue Regeneration. *Int. J. Mol. Sci.* **2020**, *21*, 3242.
(54) Li, M.; Gu, Q.; Chen, M.; Zhang, C.; Chen, S.; Zhao, J. Controlled delivery of icariin on small intestine submucosa for bone tissue engineering. *Mater. Sci. Eng., C* **2017**, *71*, 260−267.

https://doi.org/10.1021/acsomega.1c05623
ACS Omega 2021, 6, 35727−35737